JACS Au
AN OPEN ACCESS JOURNAL OF THE AMERICAN CHEMICAL SOCIETY

pubs.acs.org/jacsau

Article

Activity Self-Optimization Steered by Dynamically Evolved Fe^{3+}@Fe^{2+} Double-Center on Fe_2O_3 Catalyst for NH_3-SCR

Hai Yang Yuan, Ningning Sun, Jianfu Chen, Hua Gui Yang, P. Hu, and Haifeng Wang*

Cite This: *JACS Au* 2022, 2, 2352−2358

Read Online

ACCESS | Metrics & More | Article Recommendations | Supporting Information

ABSTRACT: Identification of the active centers dynamically stable under the reaction condition is of paramount importance but challenging because of the limited knowledge of steady-state chemistry on catalysts at the atomic level. Herein, focusing on the Fe_2O_3 catalyst for the selective catalytic reduction of NO with NH_3 (NH_3-SCR) as a model system, we reveal quantitatively the self-evolving Fe^{3+}@Fe^{2+} (∼1:1) double-centers under the in-situ condition by the first-principles microkinetic simulations, which enables the accurate prediction of the optimal industry operating temperature (590 K). The cooperation of this double-center achieves the self-optimization of catalytic activity and rationalizes the intrinsic origin of Fe_2O_3 catalyzing NH_3-SCR at middle-high temperatures instead of high temperatures. Our findings demonstrate the atomic-level self-evolution of active sites and the dynamically adjusted activity variation of the catalyst under the in-situ condition during the reaction process and provide insights into the reaction mechanism and catalyst optimization.

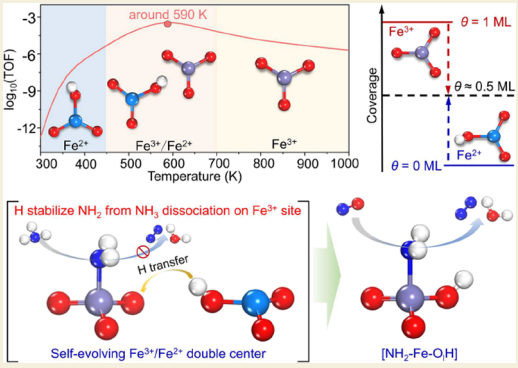

KEYWORDS: *dynamically evolving active center, activity self-optimization, reaction mechanism, NH_3-SCR, Fe_2O_3 catalyst*

INTRODUCTION

Active centers on catalysts could be dynamically changing during the in-situ reaction process and essentially determine the real catalytic activity.[1−5] To resolve how they evolve and affect the catalytic activity is critical to understand the reaction mechanism and direct the catalyst design.[6−11] However, it is very challenging to give an explicit microscopic evolution picture of active centers or accurately identify the active centers even with the advanced experimental techniques. In this respect, the determination of active sites on the reducible metal oxides has long been a typical endeavor because of their rich redox behaviors. Hereinto, Fe_2O_3 as an environmental-friendly and easily available material has drawn particular attention in the past decades. Particularly, Fe_2O_3-based catalysts exhibit superior performance at middle-high temperatures (200∼400 °C, the optimal operating one T_{opt} ≈ 600 K) instead of high temperatures for the selective catalytic reduction of NO with NH_3 (NH_3-SCR: $4NH_3 + 4NO + O_2 \rightarrow 4N_2 + 6H_2O$),[12−21] which is an advanced technology to eliminate nitrogen oxides.[22−25]

However, because of the variable valences of Fe, the issue of what are the active centers of Fe_2O_3 for NH_3-SCR is still controversial. Zhang and co-workers reported that the NO conversion is proportional to the concentration of Fe^{3+} sites,[12,16] while it was also suggested to be related with Fe^{2+} sites, as the NH_3 dissociation could reduce Fe^{3+} sites.[13,15] In principle, in the real process, Fe^{3+} and Fe^{2+} sites on the Fe_2O_3 catalyst could dynamically interconvert, which is determined by the competition between the H accumulation and removal processes and could reach a particular distribution at the steady state and affects the real NH_3-SCR activity. However, there is no general consensus on what their quantitative distribution pattern is or which one (Fe^{3+} vs Fe^{2+}) is the real active center of the Fe_2O_3 catalyst for NH_3-SCR. Fundamentally, the activity and mechanism of $Fe^{3+}$and Fe^{2+} sites for NH_3-SCR need to be clarified, including their roles in three key processes, that is, NH_3 adsorption/dissociation, NH_2NO formation/conversion, and O_2-assisted H removal (Figure 1a).[7]

Moreover, as a result of the limited mechanistic understanding and the difficulty to locate real active sites, the intrinsic origin of the balanced T_{opt} has never been explained, although abundant studies for NH_3-SCR on Fe_2O_3 catalysts have been carried out.[14−18] To provide a theoretical basis for understanding and optimizing Fe_2O_3-based catalysts for NH_3-SCR, there are three key questions to be answered: (i) What are the natural active centers of the Fe_2O_3 catalyst for NH_3-SCR? How do they dynamically evolve in the real reaction? (ii) What is the reaction mechanism of NH_3-SCR on the Fe_2O_3

Received: July 31, 2022
Revised: September 1, 2022
Accepted: September 7, 2022
Published: September 21, 2022

https://doi.org/10.1021/jacsau.2c00424
JACS Au 2022, 2, 2352−2358

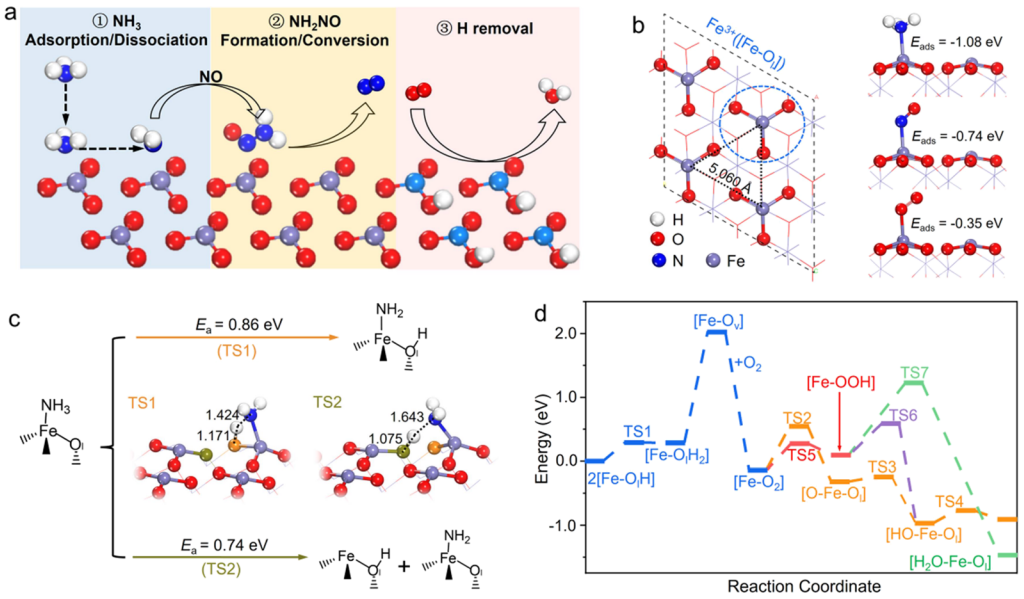

Figure 1. (a) Three main subprocesses in NH_3-SCR. (b) Top view of the optimized structure of $Fe_2O_3(001)$ and adsorption structures of NH_3, NO, and O_2 on Fe^{3+} sites, respectively. (c) Scheme for NH_3 dissociation and NH_2NO formation on the Fe^{3+} site, in which TS1 and TS2 are the transition states of NH_3 dissociation assisted by O_l from the adjacent [Fe−O_l] (orange atom) and its own of [Fe−O_l] (olive atoms), respectively. (d) Energy profile for the MvK pathway for the H removal process on $Fe_2O_3(001)$, the corresponding detailed reaction pathway are shown by Scheme S1 and the related transition states are shown in Figure S6.

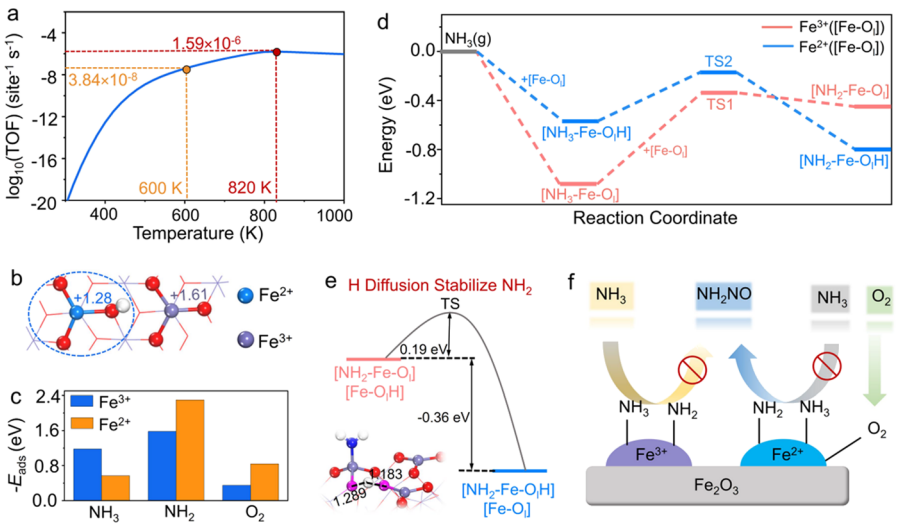

Figure 2. (a) Activity variation of NH_3-SCR on the Fe^{3+} site, where the logarithms of TOFs were plotted as a function of temperature. (b) Bader charge analysis of $Fe_2O_3(001)$ with H covered. (c) Adsorption energies of important species (NH_3, NH_2, O_2) on Fe^{3+} (blue) and Fe^{2+} sites (orange). (d) Energy profiles of NH_3 dissociation on Fe^{3+} and Fe^{2+} sites. (e) Energy of transferred H stabilizing NH_2 on the Fe^{3+} site, for example, [NH_2−Fe−O_l]@[Fe−O_lH] → [NH_2−Fe−O_lH]@[Fe−O_l]. (f) Fundamental rules of $Fe_2O_3(001)$ for catalyzing NH_3-SCR.

catalyst? (iii) What is the kinetic origin that Fe_2O_3 exhibits a superior activity around $T_{opt} \approx 600$ K?

Herein, we established a sophisticated dual-site microkinetic model with extensive density functional theory (DFT) calculations, which enables to describe the time-dependent interconversion of Fe^{3+} and Fe^{2+} sites on α-$Fe_2O_3(001)$ and incorporate systematically the elementary steps of NH_3-SCR on each site. Our results demonstrate the crucial role of dynamic evolving Fe^{3+}@Fe^{2+} double-centers that can interestingly achieve the self-optimization of catalytic activity of Fe_2O_3 and rationalize the origin of its superior activity for NH_3-SCR at middle-high temperatures, while the single Fe^{3+} sites on the pristine Fe_2O_3 catalyst cannot correctly describe the reaction behavior of NH_3-SCR.

RESULTS AND DISCUSSION

Mechanism and Activity on Fe^{3+} Sites for NH_3-SCR

To begin with, we carried out systematic DFT calculations to explore the mechanism of NH_3-SCR on the α-$Fe_2O_3(001)$ surface. $Fe_2O_3(001)$ is terminated by unsaturated Fe^{3+} sites bound by three lattice oxygens (O_l) as shown in Figure 1b, which constitute the initial active centers. The distance between two adjacent Fe sites is long (5.060 Å), showing that each Fe site is isolated as a [Fe−O_l] unit (Figure 1b), and one can thus speculate that the direct intermediate diffusion

https://doi.org/10.1021/jacsau.2c00424
JACS Au 2022, 2, 2352−2358

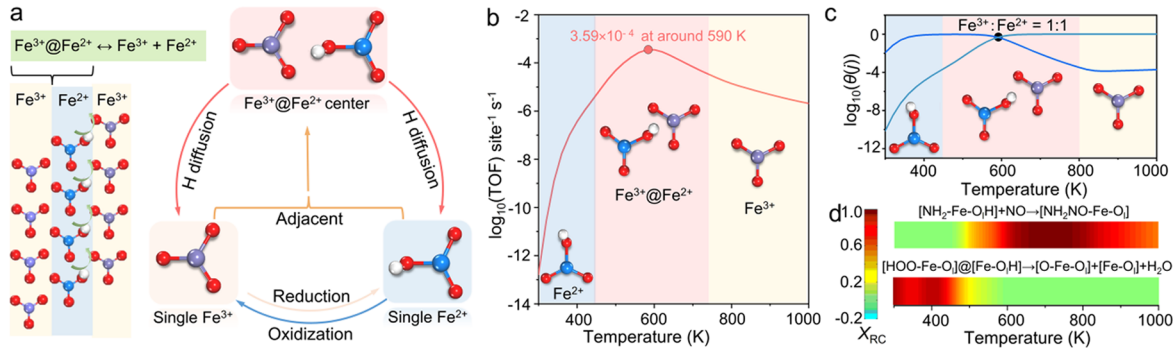

Figure 3. (a) Microkinetic model diagram of NH_3-SCR on the Fe_2O_3 surface. (b) Active trend of NH_3-SCR on the Fe_2O_3 catalyst, in which the logarithm of TOF was plotted as a function of temperature. (c) Coverage trends of Fe^{3+} and Fe^{2+}sites on Fe_2O_3, in which the logarithm of coverages was plotted as a function of temperature. (d) Variation of the degree of rate control (X_{RC}) of different rate-limiting steps as a function of temperature.

among Fe sites could be inhibited. First, on the pristine $Fe_2O_3(001)$, Fe^{3+} sites prefer to bond with NH_3 ($[NH_3{-}Fe{-}O_l]$) instead of the other two reactants NO and O_2 (E_{ads} = −1.18 eV vs −0.74 eV vs −0.35 eV, Figure 1b), indicating that NH_3 activation on the Fe^{3+} site is the starting step to trigger NH_3-SCR. As shown in Figure 1c, we identified that in the NH_3 dissociation, $[NH_3{-}Fe{-}O_l]$ kinetically tends to dissociate by O_l on the adjacent $[Fe{-}O_l]$ unit instead of its own O_l:

$$[NH_3 - Fe - O_l] + [Fe - O_l] \rightarrow [NH_2 - Fe - O_l]@[Fe - O_lH],\ E_a = 0.74\ eV \quad (R1)$$

$$[NH_3 - Fe - O_l] \rightarrow [NH_2 - Fe - O_lH],\ E_a = 0.86\ eV \quad (R2)$$

This implies that the adjacent $[Fe{-}O_l]$ unit is favored to break the N−H bond in $*NH_3$, which can be ascribed to more matched bonding orientation and thus the less sterically strained $NH_2{\cdots}H{\cdots}O_l$ bond at the transition state (see TS2 vs TS1 in Figure 1c). Notably, the further decomposition of $*NH_2$ is unfavorable due to the substantially increased effective barrier of the overall process (Figure S2). Second, the formed $*NH_2$ can couple with the gaseous NO to form NH_2NO (ΔH = −2.38 eV, Figure S4), which is a key intermediate fulfilling the N−N bond linkage and can further convert into N_2 and H_2O easily by the hydrogen push−pull mechanism (Figure S5).[7,26,27] Third, for weak O_2 adsorption on the Fe^{3+} site (E_{ads} = −0.35 eV), the removal of H species from $Fe_2O_3(001)$ preferentially follows the Mars-van Krevelen pathway (MvK, Figure 1d).[7,26] More details for the NH_3-SCR process on the pristine $Fe_2O_3(001)$ are discussed in Notes S1−S3.

With the energetic data on Fe^{3+} site, the activity trend of NH_3-SCR on the pristine $Fe_2O_3(001)$ surface at different temperatures (300 K < T < 1000 K) was examined by the kinetic simulation (Figure 2a, see method details in Note S4). The results show that the N_2 formation rate can reach the optimal value (~10^{-6} site^{-1} s^{-1}) only at a high temperature of ~820 K, which does not conform to the real middle-high temperature of ~600 K in experiments.[14−18] At 600 K, the N_2 formation rate on the pristine Fe_2O_3 is low, only 3.84 × 10^{-8} site^{-1} s^{-1}, implying that NH_3-SCR is hardly catalyzed at middle-high temperatures by Fe_2O_3 with only Fe^{3+} sites. The origin of such a low rate can be traced to difficult coupling of NO and $*NH_2$ on the Fe^{3+} site from the microkinetic simulation (Note S5).

NH_3-SCR on $Fe_2O_3(001)$ with Fe^{2+} Sites Involved

In the realistic NH_3-SCR, the presence of H species from NH_3 dissociation and NH_2NO conversion could reduce Fe^{3+} sites to Fe^{2+} ones (i.e., $[Fe{-}O_l] \rightarrow [Fe{-}O_lH]$),[13,15] as verified by the Bader charge analysis (Figure 2b). Then, the NH_3-SCR process on the Fe^{2+} site was also examined. In comparison with the Fe^{3+} site, although the NH_3 dehydrogenation on Fe^{2+} assisted by adjacent $[Fe{-}O_l]$ is easier at a lower barrier (E_a = 0.40 eV) and becomes thermodynamically favorable (Figure 2d), the adsorption of NH_3 on the Fe^{2+} site becomes much weaker (E_{ads} = −1.18 eV vs −0.57 eV, Figure 2c). Thus, the NH_3 dehydrogenation on Fe^{2+} sites could be unfeasible compared with that on Fe^{3+} sites kinetically. Nevertheless, there is a much-enhanced NH_2 bonding on the Fe^{2+} site ($[NH_2{-}Fe{-}O_lH]$) than on the Fe^{3+} one (E_{ads} = −2.35 eV vs −1.58 eV, Figure 2c). This implies that the $[NH_2{-}Fe{-}O_l]$ intermediate could be stabilized into $[NH_2{-}Fe{-}O_lH]$ if H species diffusion can occur ($[NH_2{-}Fe{-}O_l] + [Fe{-}O_lH] \rightarrow [NH_2{-}Fe{-}O_lH] + [Fe{-}O_l]$), which corresponds to a stabilization energy of $\Delta G_s(H)$ = −0.36 eV. Moreover, this H diffusion to stabilize NH_2 only needs to overcome a low barrier of 0.19 eV (Figure 2e). These results support the feasible formation of $[NH_2{-}Fe{-}O_lH]$, facilitating the $*NH_2$ and NO coupling step by increasing the coverage of NH_2. In addition, the O_2 adsorption on the Fe^{2+} site is also promoted compared with that on the Fe^{3+} site (E_{ads} = −0.84 eV vs −0.35 eV), which can create a new feasible H removal pathway, that is, the Langmuir−Hinshelwood (L-H) pathway (Figure S7), promoting the H removal process.

By comparing the above energetics on the Fe^{3+} and Fe^{2+} sites, we can find some fundamental rules on the Fe_2O_3 catalyst for NH_3-SCR (Figure 2f): (i) the Fe^{3+} site is preferred for the NH_3 adsorption and dissociation into $*NH_2$ but is unfavoured for converting $*NH_2$ into NH_2NO and capturing O_2 for H species removal and (ii) the Fe^{2+} site helps stabilize NH_2 and contributes to NH_2NO formation, and promotes O_2 adsorption and thus the H removal process by the L-H pathway.

Kinetic Analysis on the Fe^{3+}@Fe^{2+} Double-Center

Under the in situ condition, the Fe^{3+} and Fe^{2+} sites on Fe_2O_3 can be interconverted by H accumulation and removal, leading to the complicated distribution of Fe^{3+} and Fe^{2+} sites. It is challenging to quantitatively determine their coverage and catalytic contribution. Because of the limitation of the traditional microkinetic model in describing dynamically varied

https://doi.org/10.1021/jacsau.2c00424
JACS Au 2022, 2, 2352−2358

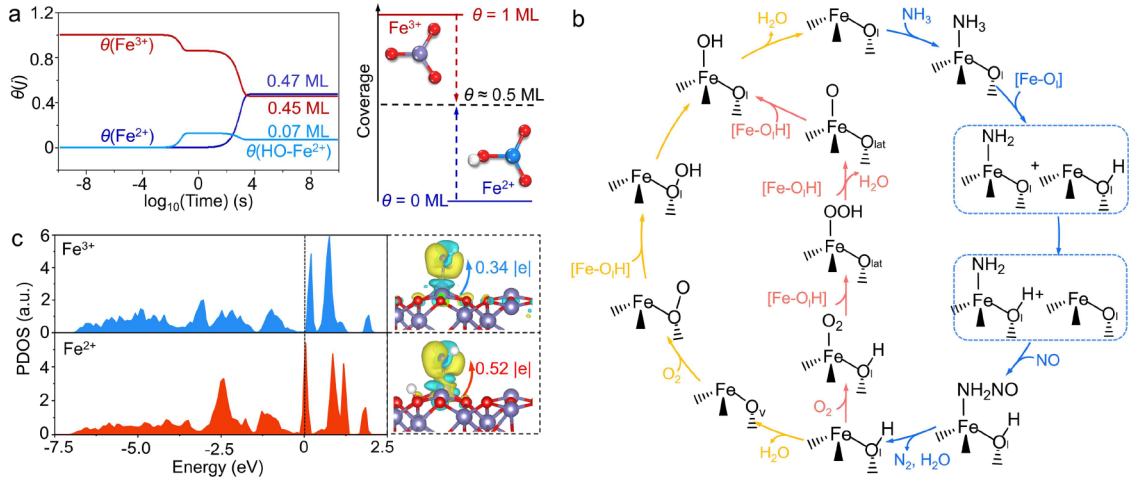

Figure 4. (a) Coverage trends of the main species in NH_3-SCR. (b) Mechanism of NH_3-SCR on the Fe^{3+}@Fe^{2+} double-center. (c) Projected densities of states (PDOS) of the *d* orbital for the Fe^{3+} and Fe^{2+} sites, and the charge density difference of NH_2 on Fe^{3+} and Fe^{2+} sites, in which yellow and green indicate the electron accumulation and depletion, respectively.

active centers on catalysts surface, here, we constructed a dual-site microkinetic model for NH_3-SCR on the Fe_2O_3 catalyst, which can describe the variations of Fe^{3+} and Fe^{2+} active sites during the reaction process. Specifically, as illustrated in Figure 3a, this kinetic model for NH_3-SCR on the Fe_2O_3 catalyst contains the following features. (i) This model regards the isolated Fe^{3+} or Fe^{2+} sites as two individual active sites for NH_3-SCR and particularly allows the adjacent Fe^{3+} and Fe^{2+} sites as an effective unit (donated as [Fe−O_l]@[Fe−O_lH]). This approach can provide the way to describe the reaction steps occurring on the dual sites, especially for the elementary step with the variable active sites involved, for example, [NH_2−Fe−O_l]@[Fe−O_lH] → [NH_2−Fe−O_lH]@[Fe−O_l]. (ii) The H species diffusion event between the lattice O is explicitly included, while the direct species diffusion between Fe^{3+} and Fe^{2+} sites is prevented because of the long distance between them. (iii) When H species in [Fe−O_l]@[Fe−O_lH] is diffused away, the [Fe−O_l]@[Fe−O_lH] unit converts into the individual Fe^{2+} and Fe^{3+} ones (i.e., [Fe−O_l]@[Fe−O_lH] → [Fe−O_l] + [Fe−O_lH]); such a strategy helps to achieve the self-regulation of the distributions of Fe^{2+} and Fe^{3+} sites and their synergy. Accordingly, we constructed the NH_3-SCR microkinetic model on Fe_2O_3 (Table S4) and explored the activity trend of NH_3-SCR on Fe_2O_3 at different temperatures (300 K < *T* < 1000 K, see details in Note S6).

As shown in Figure 3b, Fe_2O_3 reaches the maximum activity at the temperature of 590 K. It should be emphasized that this predicted optimal temperature well agrees with the optimum experimental temperature range (~600 K) for NH_3-SCR on Fe_2O_3-based catalysts.[12−21] Around this optimal temperature (T_{opt} = 590 K), the ratio of $\theta(Fe^{3+})$ and $\theta(Fe^{2+})$ approaches about 1:1 at the steady state (Figure 3c), illustrating the existence of Fe^{3+}@Fe^{2+} double-centers on the Fe_2O_3 catalyst in NH_3-SCR. Noticeably, with the Fe^{3+}@Fe^{2+} double-center involved, the obtained reaction rate (3.59×10^{-4} site^{-1} s^{-1}) is well consistent with the rate reported in the experiment (~10^{-4} site^{-1} s^{-1}).[12]

To further probe the self-evolution of Fe^{3+}@Fe^{2+} double-centers, we carried out the time-dependent ODE (ordinary differential equation) simulation of NH_3-SCR on Fe_2O_3 at 590 K. As can be seen from Figure 4a, as NH_3-SCR proceeds from *t* = 0 s, the surface Fe^{3+} sites are gradually reduced by the H species to Fe^{2+} sites, resulting in the decrease of $\theta(Fe^{3+})$ (≈0.9 ML) at about *t* = 0.09 s; at this time, the reaction reaches the second steady state, and the formed Fe^{2+} sites are covered by OH species. As NH_3-SCR further progresses to *t* = 4.0 s, the surface Fe^{3+} sites are reduced to Fe^{2+} sites, and the reaction reaches the final steady state at *t* = 1000 s, which corresponds to the presence of the induction period. Under this final steady state condition, about half Fe^{3+} sites are reduced to Fe^{2+} ones, showing the existence of Fe^{3+}@Fe^{2+} double-centers ($\theta(Fe^{3+})$ = 0.45 ML, $\theta(Fe^{2+})$ = 0.47 ML) and demonstrating that the self-evolving Fe^{3+}@Fe^{2+} double-centers are the real active sites of the Fe_2O_3 catalyst for NH_3-SCR.

After comparing the rate of each elementary step of NH_3-SCR on Fe_2O_3 at the optimal temperature of 590 K (Table S4), we can ascertain the real NH_3-SCR mechanism on the Fe_2O_3(001) catalyst with the Fe^{3+}@Fe^{2+} double-center involved (Figure 4b). First, NH_3 prefers to adsorb and dissociate into *NH_2 on the Fe^{3+} site, while the adjacent Fe^{2+} unit tends to transfer the H back to [NH_2−Fe−O_l]; such a back-and-forth shuttling mechanism ensures a low-barrier process and stabilizes *NH_2, largely contributing to the NH_2NO formation. Second, NH_2NO easily converts into N_2 and H_2O, following the hydrogen push−pull mechanism on the Fe^{2+} site. Third, by virtue of the Fe^{2+} site, O_2 adsorption can be enhanced and constitute an alternative L-H pathway in addition to the dominant MvK pathway to remove H species from the surface. The energy profile for the optimal mechanism is shown in Figure S10. Following this mechanism, the NO elimination rate can reach a maximum value of 3.59×10^{-4} site^{-1} s^{-1} at T_{opt} = 590 K, which is nearly 10^2 times the optimal one at about 820 K (vs 1.59×10^{-6} site^{-1} s^{-1}) and 10^4 times larger than that at experimental temperature 600 K (vs 3.84×10^{-8} site^{-1} s^{-1}) on the pristine Fe_2O_3(001) surface. These results indicate that, with the self-evolution of Fe^{3+}@Fe^{2+} double-center of Fe_2O_3, its activity can be self-promoted, and the reaction condition is self-adjusted to lower operating temperature.

Origins of the Self-Optimized Performance of the Fe^{3+}@Fe^{2+} Double-Center for NH_3-SCR

Now, a remaining question is to resolve the intrinsic origin of the self-optimizing reaction condition and activity on the Fe^{3+}@Fe^{2+} double-center. To this end, we conducted the

https://doi.org/10.1021/jacsau.2c00424
JACS Au 2022, 2, 2352−2358

degree of rate control (X_{RC}) analysis, and found that the *NH_2 and NO coupling step is always rate-determining on either Fe^{3+} sites or Fe^{3+}@Fe^{2+} double-centers at middle-high temperatures (Figure 3d, see details in Notes S5 and S6). The energy profile of NH_3-SCR also verifies that the transition state of *NH_2 and NO coupling step locates at the highest position (Figure S11). Therefore, the effective barrier, which determines the overall rate of NH_3-SCR on the Fe^{3+} site and Fe^{3+}@Fe^{2+} double-center, can be respectively written as follows:

$$E_a(Fe^{3+}) = \Delta G_{dis}(NH_3 \rightarrow NH_2) + E_a(NH_2NO) \quad (1)$$

$$E_a(Fe^{3+}@Fe^{2+}) = \Delta G_{dis}(NH_3 \rightarrow NH_2) + \Delta G_s(H) + E_a(NH_2NO) \quad (2)$$

where $E_a(NH_2NO)$ is the barrier of *NH_2 coupling with NO, and $\Delta G_s(H)$ is the stabilization energy for *NH_2 on the Fe^{3+}@Fe^{2+} double-center relative to the Fe^{3+} site. $\Delta G_{dis}(NH_3 \rightarrow NH_2)$ is the free energy change of NH_3 adsorption/dissociation on the Fe^{3+} site:

$$\Delta G_{dis}(NH_3 \rightarrow NH_2) = G_{ads}(NH_3) + \Delta H_{dis}(^*NH_3 \rightarrow NH_2) = E_{ads}(NH_3) - T^*S + \Delta H_{dis}(^*NH_3 \rightarrow NH_2) \quad (3)$$

in which $G_{ads}(NH_3)$ is the adsorption free energy of NH_3, S is the entropy of the NH_3 molecule at given T, and $\Delta H_{dis}(^*NH_3 \rightarrow NH_2)$ is the enthalpy change of *NH_3 dissociation on the Fe^{3+} sites. Accordingly, by comparing $E_a(Fe^{3+})$ and $E_a(Fe^{3+}@Fe^{2+})$, one can obtain the main determining factors behind their difference:

$$E_a(Fe^{3+}) - E_a(Fe^{3+}@Fe^{2+}) = T^*S(Fe^{3+}@Fe^{2+}) - T^*S(Fe^{3+}) - \Delta G_s(H) \quad (4)$$

The following insights are evident by analyzing these equations: (i) At a given temperature, $E_a(Fe^{3+})$ is larger than $E_a(Fe^{3+}@Fe^{2+})$ because of the presence of the negative $\Delta G_s(H)$ term (−0.36 eV), thus leading to the self-promoting NH_3-SCR activity of Fe^{3+}@Fe^{2+} double-center relative to that of Fe^{3+} sites. (ii) When $E_a(Fe^{3+})$ is equal to $E_a(Fe^{3+}@Fe^{2+})$, the lower temperature is required for NH_3-SCR on Fe^{3+}@Fe^{2+} double-centers, that is, $T^*S(Fe^{3+}@Fe^{2+}) < T^*S(Fe^{3+})$. It is clear that the $\Delta G_s(H)$ term on the self-evolving Fe^{3+}@Fe^{2+}double-center, that is the stabilization of *NH_2 on the Fe^{3+} site by the electron-donating effect of H transferred from the adjacent Fe^{2+} sites that results in the higher-energy-level electron (Figure 4c), is the intrinsic origin of Fe_2O_3 with self-optimized activity at lower temperatures instead of high temperatures in the realistic NH_3-SCR.

CONCLUSIONS

In summary, we explored the dynamic evolution of the active centers of the Fe_2O_3 catalyst for NH_3-SCR and quantitatively revealed the self-evolving Fe^{3+}@Fe^{2+} double-center under the in-situ condition. With the cooperation of the Fe^{3+}@Fe^{2+} double-center, the catalytic activity and reaction temperature of Fe_2O_3 for NH_3-SCR can be self-optimized; the predicted optimal operating temperature (590 K) is perfectly in accordance with the adopted condition (~600 K) in industry. More importantly, the intrinsic origin of the self-promotion effect of this Fe^{3+}@Fe^{2+} double-center for NH_3-SCR was rationalized, in which the Fe^{2+} site largely stabilizes *NH_2 from the NH_3 dissociation on the Fe^{3+} site, accelerating the rate-determining NH_2NO formation. Beyond the usually relatively "macroscopic" observations for catalyst's dynamic evolution, such as the particle growth, morphology variation, and reconstruction, this work demonstrates an atomic-level self-evolution of active centers and the dynamically adjusted activity variation under the in-situ condition, which could not only provide a fundamental understanding of the catalytic mechanism but also be a key to optimize catalysts for the reaction.

METHODS

DFT Calculation Method

The spin-polarized density functional calculation, using the Perdew–Burke–Ernzerhof (PBE) functional win the generalized gradient approximation (GGA),[28] was performed with the Vienna ab initio simulation package (VASP).[29] The electron-ion interaction was treated with the projector-augmented wave (PAW) method,[30] and the valence electronic states were expanded in a plane-wave cutoff energy of 450 eV. The Broyden method was employed for geometry optimization until the force on each atom of the model was less than 0.05 eV/Å. α-Fe_2O_3 (hematite) is crystallized in the hexagonal structure (see Figure S1a), and the (001) surface as the growing surface is usually one of the most exposed and active facets,[31−33] which was thus selected to explore the NH_3-SCR process on α-Fe_2O_3 catalysts. The α-Fe_2O_3 (001) surface was modeled by a 12-layer slab model with a vacuum of 15 Å in the z-direction. During the structural optimization, the bottom six layers were fixed, and the top six layers and the adsorbates on surface were completely relaxed. Correspondingly, a 2 × 1 × 1 k-point mesh was used. The constrained optimization scheme was used to search the transition states.[34] To well describe the strongly correlated Fe-3d electrons of α-Fe_2O_3, the DFT + U approach with the on-site Coulomb correction included was used. A Hubbard-like term U_{eff} = 4.0 eV (U = 5.0 eV and J = 1.0 eV) for Fe (3d) was adopted, which could reproduce the bulk lattice parameter band gap and magnet moment of α-Fe_2O_3.[35−37] Additionally, it has been noted that α-Fe_2O_3 is the antiferromagnetic state; thus, an antiferromagnetic helical spin arrangement ("+ + − −") was adopted in our calculation (see Figure S1b), where "+" and "−" represent spin up and spin down, respectively.[37,38] The adsorption energies of adsorbates were calculated with $E_{ads}(X) = E_{x/surf} - E_{surf} - E_x$, where E_x, E_{surf}, and $E_{x/surf}$ are the total energies of adsorbates (X) in the gas phase, the clean surface, and the optimized surface with adsorbed X, respectively. The more negative E_{ads} means the stronger interaction between X and the surface.

Dual-Site Microkinetic Model

The traditional microkinetic model focuses on the single-site system,[39,40] in which the species diffusions are considered as fast steps and not explicitly involved and can hardly describe the catalytic system with dynamically varied active centers. Here, we proposed a dual-site microkinetic model, which can describe the variations of active sites during the reaction process. In this microkinetic model, except for the common isolated active centers on catalyst, the active center pair constituted by different active sites, for example, Fe^{3+}@Fe^{2+} double-center reported here, can also be considered, which helps describe the reaction steps occurring on the dual-sites, especially for the synergetic role with the variable active sties involved. The specific dual-site microkinetic model for NH_3-SCR on the Fe_2O_3 catalyst is discussed in detail in the main text and Supporting Information. Here, the microkinetic simulation was carried out with our developed CATKINAS package,[41−43] in which the free energy change (ΔG) of each elementary step was considered. In the microkinetic analysis, the entropy effects have been considered to estimate the Gibbs free energy change (ΔG) of the elementary step according to $\Delta G = \Delta H - T\Delta S$. Regarding the entropy effect term ($T\Delta S$), for the surface

https://doi.org/10.1021/jacsau.2c00424
JACS Au 2022, 2, 2352−2358

reactions with no adsorption/desorption, the entropies of the surface species are typically small and can also be largely canceled between the initial state and the transition state or the final state;[44−46] for the adsorption/desorption processes, the large entropy contribution of gaseous molecules ($T\Delta S$), including the vibrational, rotational, and translational entropies, have to be considered to estimate ΔG at a given temperature, which were obtained with the experimental values.[47]

■ ASSOCIATED CONTENT

Supporting Information

The Supporting Information is available free of charge at https://pubs.acs.org/doi/10.1021/jacsau.2c00424.

Structures of intermediates and transition states in NH_3-SCR; method of microkinetic simulation; and detailed discussion for NH_3-SCR on the Fe_2O_3 catalyst (PDF)

■ AUTHOR INFORMATION

Corresponding Author

Haifeng Wang − *Key Laboratory for Advanced Materials and Joint International Research Laboratory of Precision Chemistry and Molecular Engineering, Feringa Nobel Prize Scientist Joint Research Center, Research Institute of Industrial Catalysis and Centre for Computational Chemistry, School of Chemistry and Molecular Engineering, East China University of Science and Technology, Shanghai 200237, P. R. China;* orcid.org/0000-0002-6138-5800; Email: hfwang@ecust.edu.cn

Authors

Hai Yang Yuan − *Key Laboratory for Advanced Materials and Joint International Research Laboratory of Precision Chemistry and Molecular Engineering, Feringa Nobel Prize Scientist Joint Research Center, Research Institute of Industrial Catalysis and Centre for Computational Chemistry, School of Chemistry and Molecular Engineering, East China University of Science and Technology, Shanghai 200237, P. R. China; Key Laboratory for Ultrafine Materials of Ministry of Education, Shanghai Engineering Research Center of Hierarchical Nanomaterials, School of Materials Science and Engineering, East China University of Science and Technology, Shanghai 200237, China*

Ningning Sun − *Key Laboratory for Advanced Materials and Joint International Research Laboratory of Precision Chemistry and Molecular Engineering, Feringa Nobel Prize Scientist Joint Research Center, Research Institute of Industrial Catalysis and Centre for Computational Chemistry, School of Chemistry and Molecular Engineering, East China University of Science and Technology, Shanghai 200237, P. R. China*

Jianfu Chen − *Key Laboratory for Advanced Materials and Joint International Research Laboratory of Precision Chemistry and Molecular Engineering, Feringa Nobel Prize Scientist Joint Research Center, Research Institute of Industrial Catalysis and Centre for Computational Chemistry, School of Chemistry and Molecular Engineering, East China University of Science and Technology, Shanghai 200237, P. R. China*

Hua Gui Yang − *Key Laboratory for Ultrafine Materials of Ministry of Education, Shanghai Engineering Research Center of Hierarchical Nanomaterials, School of Materials Science and Engineering, East China University of Science and Technology, Shanghai 200237, China;* orcid.org/0000-0003-0436-8622

P. Hu − *Key Laboratory for Advanced Materials and Joint International Research Laboratory of Precision Chemistry and Molecular Engineering, Feringa Nobel Prize Scientist Joint Research Center, Research Institute of Industrial Catalysis and Centre for Computational Chemistry, School of Chemistry and Molecular Engineering, East China University of Science and Technology, Shanghai 200237, P. R. China; School of Chemistry and Chemical Engineering, The Queen's University of Belfast, Belfast BT9, U.K.;* orcid.org/0000-0002-6318-1051

Complete contact information is available at: https://pubs.acs.org/10.1021/jacsau.2c00424

Notes

The authors declare no competing financial interest.

■ ACKNOWLEDGMENTS

This project was supported by the National Key Research and Development Program of China (2021YFA1500700), the National Natural Science Foundation of China (91945302, 92045303, 21902048, 21873028), the National Ten Thousand Talent Program for Young Top-notch Talents in China, and the Fundamental Research Funds for the Central Universities.

■ REFERENCES

(1) Ding, K.; Gulec, A.; Johnson, A. M.; Schweitzer, N. M.; Stucky, G. D.; Marks, L. D.; Stair, P. C. Identification of active sites in CO oxidation and water-gas shift over supported Pt catalysts. *Science* **2015**, *350*, 189−192.

(2) Yuan, W.; Zhu, B.; Fang, K.; Li, X. Y.; Hansen, T. W.; Ou, Y.; Yang, H.; Wagner, J. B.; Gao, Y.; Wang, Y.; Zhang, Z. In situ manipulation of the active Au-TiO_2 interface with atomic precision during CO oxidation. *Science* **2021**, *371*, 517−521.

(3) Mefford, J. T.; Akbashev, A. R.; Kang, M.; Bentley, C. L.; Gent, W. E.; Deng, H. D.; Alsem, D. H.; Yu, Y. S.; Salmon, N. J.; Shapiro, D. A.; Unwin, P. R.; Chueh, W. C. Correlative operando microscopy of oxygen evolution electrocatalysts. *Nature* **2021**, *593*, 67−73.

(4) Barroo, C.; Wang, Z. J.; Schlögl, R.; Willinger, M. G. Imaging the dynamics of catalysed surface reactions by in situ scanning electron microscopy. *Nat. Catal.* **2020**, *3*, 30−39.

(5) Yan, G.; Tang, Y.; Li, Y.; Li, Y.; Nguyen, L.; Sakata, T.; Higashi, K.; Tao, F. F.; Sautet, P. Reaction product-driven restructuring and assisted stabilization of a highly dispersed Rh-on-ceria catalyst. *Nat. Catal.* **2022**, *5*, 119−127.

(6) Lien, H. T.; Chang, S. T.; Chen, P. T.; Wong, D. P.; Chang, Y. C.; Lu, Y. R.; Dong, C. L.; Wang, C. H.; Chen, K. H.; Chen, L. C. Probing the active site in single-atom oxygen reduction catalysts via operando X-ray and electrochemical spectroscopy. *Nat. Commun.* **2020**, *11*, 4233.

(7) Yuan, H.; Sun, N.; Chen, J.; Jin, J.; Wang, H.; Hu, P. Insight into the NH_3-assisted selective catalytic reduction of NO on β-MnO_2(110): reaction mechanism, activity descriptor, and evolution from a pristine state to a steady state. *ACS Catal.* **2018**, *8*, 9269−9279.

(8) Li, J.; Gong, J. Operando characterization techniques for electrocatalysis. *Energy Environ. Sci.* **2020**, *13*, 3748−3779.

(9) Qu, W.; Liu, X.; Chen, J.; Dong, Y.; Tang, X.; Chen, Y. Single-atom catalysts reveal the dinuclear characteristic of active sites in NO selective reduction with NH3. *Nat. Commun.* **2020**, *11*, 1532.

(10) Liu, B.; Liu, J.; Xin, L.; Zhang, T.; Xu, Y.; Jiang, F.; Liu, X. Unraveling reactivity descriptors and structure sensitivity in low-temperature NH3-SCR reaction over CeTiOx catalysts: a combined computational and experimental study. *ACS Catal.* **2021**, *11*, 7613−7636.

(11) Millan, R.; Cnudde, P.; Van Speybroeck, V.; Boronat, M. Mobility and reactivity of Cu^+ species in Cu-CHA catalysts under NH_3-SCR-NO_x reaction conditions: insights from AIMD simulations. *JACS Au* **2021**, *1*, 1778−1787.
(12) Liu, J.; Meeprasert, J.; Namuangruk, S.; Zha, K.; Li, H.; Huang, L.; Maitarad, P.; Shi, L.; Zhang, D. Facet-activity relationship of TiO2 in Fe2O3/TiO2 nanocatalysts for selective catalytic reduction of NO with NH3: in situ DRIFTs and DFT studies. *J. Phys. Chem. C* **2017**, *121*, 4970−4979.
(13) Apostolescu, N.; Geiger, B.; Hizbullah, K.; Jan, M. T.; Kureti, S.; Reichert, D.; Schott, F.; Weisweiler, W. Selective catalytic reduction of nitrogen oxides by ammonia on iron oxide catalysts. *Appl. Catal. B-Environ.* **2006**, *62*, 104−114.
(14) Mou, X.; Zhang, B.; Li, Y.; Yao, L.; Wei, X.; Su, D. S.; Shen, W. Rod-shaped Fe_2O_3 as an efficient catalyst for the selective reduction of nitrogen oxide by ammonia. *Angew. Chem., Int. Ed.* **2012**, *51*, 2989−2993.
(15) Yang, S.; Li, J.; Wang, C.; Chen, J.; Ma, L.; Chang, H.; Chen, L.; Yan, N. Fe-Ti spinel for the selective catalytic reduction of NO with NH_3: mechanism and structure−activity relationship. *Appl. Catal. B-Environ.* **2012**, *117*, 73−80.
(16) Yang, S.; Liu, C.; Chang, H.; Ma, L.; Qu, Z.; Yan, N.; Wang, C.; Li, J. Improvement of the activity of γ-Fe2O3 for the selective catalytic reduction of NO with NH3 at high temperatures: NO reduction versus NH3 oxidization. *Ind. Eng. Chem. Res.* **2013**, *52*, 5601−5610.
(17) Xie, C.; Zhu, B.; Sun, Y. A DFT-D study on the reaction mechanism of selective catalytic reduction of NO by NH3 over the Fe2O3/Ni(111) surface. *New J. Chem.* **2021**, *45*, 6458−6468.
(18) Gao, M.; He, G.; Zhang, W.; Du, J.; He, H. Reaction pathways of the selective catalytic reduction of NO with NH3 on the α-Fe2O3(012) surface: a combined experimental and DFT study. *Environ. Sci. Technol.* **2021**, *55*, 10967−10974.
(19) Han, J.; Meeprasert, J.; Maitarad, P.; Nammuangruk, S.; Shi, L.; Zhang, D. Investigation of the facet-dependent catalytic performance of Fe2O3/CeO2 for the selective catalytic reduction of NO with NH3. *J. Phys. Chem. C* **2016**, *120*, 1523−1533.
(20) Zhang, W.; Shi, X.; Yan, Z.; Shan, Y.; Zhu, Y.; Yu, Y.; He, H. Design of high-performance ion-niobium composite oxide catalysts for NH3-SCR: insights into the interaction between Fe and Nb. *ACS Catal.* **2021**, *11*, 9825−9836.
(21) Gong, Z.; Niu, S. L.; Zhang, Y. J.; Lu, C. M. Facile synthesis of porous α-Fe_2O_3 nanostructures from MIL-100(Fe) via sacrificial templating method, as efficient catalysts for NH_3-SCR reaction. *Mater. Res. Bull.* **2020**, *123*, 110693.
(22) Lian, Z.; Wei, J.; Shan, W.; Yu, Y.; Radjenovic, P. M.; Zhang, H.; He, G.; Liu, F.; Li, J. F.; Tian, Z. Q.; He, H. Adsorption-induced active vanadium species facilitate excellent performance in low-temperature catalytic NOx abatement. *J. Am. Chem. Soc.* **2021**, *143*, 10454−10461.
(23) Negri, C.; Selleri, T.; Borfecchia, E.; Martini, A.; Lomachenko, K. A.; Janssens, T. V.; Cutini, M.; Bordiga, S.; Berlier, G. Structure and reactivity of oxygen-bridged diamino dicopper (II) complexes in Cu-ion-exchanged chabazite catalyst for NH3-mediated selective catalytic reduction. *J. Am. Chem. Soc.* **2020**, *142*, 15884−15896.
(24) Hu, W.; Selleri, T.; Gramigni, F.; Fenes, E.; Rout, K. R.; Liu, S.; Nova, I.; Chen, D.; Gao, X.; Tronconi, E. On the redox mechanism of low-temperature NH_3-SCR over Cu-CHA: a combined experimental and theoretical study of the reduction half cycle. *Angew. Chem., Int. Ed.* **2021**, *60*, 7197−7204.
(25) Ryu, T.; Ahn, N. H.; Seo, S.; Cho, J.; Kim, H.; Jo, D.; Park, G. T.; Kim, P. S.; Kim, C. H.; Bruce, E. L.; Wright, P. A.; Nam, I. S.; Hong, S. B. Fully copper-exchanged high-silica LTA zeolites as unrivaled hydrothermally stable NH3-SCR catalysts. *Angew. Chem., Int. Ed.* **2017**, *129*, 3304−3308.
(26) Mao, Y.; Wang, Z.; Wang, H. F.; Hu, P. Understanding catalytic reactions over zeolites: A density functional theory study of selective catalytic reduction of NOx by NH3 over Cu-SAPO-34. *ACS Catal.* **2016**, *6*, 7882−7891.
(27) Yang, M.; Yuan, H.; Wang, H.; Hu, P. Insights into the selective catalytic reduction of NO by NH_3 over Mn_3O_4(110): a DFT study coupled with microkinetic analysis. *Sci. China Chem.* **2018**, *61*, 457−467.
(28) Perdew, J. P.; Ruzsinszky, A.; Csonka, G. I.; Vydrov, O. A.; Scuseria, G. E.; Constantin, L. A.; Zhou, X.; Burke, K. Restoring the density-gradient expansion for exchange in solids and surfaces. *Phys. Rev. Lett.* **2008**, *100*, No. 136406.
(29) Kresse, G.; Furthmüller, J. Efficient iterative schemes for ab initio total-energy calculations using a plane-wave basis set. *Phys. Rev. B* **1996**, *54*, 11169−11186.
(30) Kresse, G.; Joubert, D. From ultrasoft pseudopotentials to the projector augmented-wave method. *Phys. Rev. B* **1999**, *59*, 1758−1775.
(31) Weiss, W.; Ranke, W. Surface chemistry and catalysis on well-defined epitaxial iron-oxide layers. *Prog. Surf. Sci.* **2002**, *70*, 1−151.
(32) Qiao, B.; Wang, A.; Yang, X.; Allard, L. F.; Jiang, Z.; Cui, Y.; Liu, J.; Li, J.; Zhang, T. Single-atom catalysis of CO oxidation using Pt_1/FeO_x. *Nat. Chem.* **2011**, *3*, 634−641.
(33) Yin, S.; Ma, X.; Ellis, D. E. Initial stages of H_2O adsorption and hydroxylation of Fe-terminated α-Fe_2O_3(0001) surface. *Surf. Sci.* **2007**, *601*, 2426−2437.
(34) Alavi, A.; Hu, P.; Deutsch, T.; Silvestrelli, P. L.; Hutter, J. CO oxidation on Pt (111): an ab initio density functional theory study. *Phys. Rev. Lett.* **1998**, *80*, 3650−3653.
(35) Dudarev, S. L.; Botton, G. A.; Savrasov, S. Y.; Humphreys, C. J.; Sutton, A. P. Electron-energy-loss spectra and the structural stability of nickel oxide: An LSDA+ U study. *Phys. Rev. B* **1998**, *57*, 1505.
(36) Fang, Q.; Zhu, B.; Sun, Y.; Zhu, Z.; Xu, M.; Ge, T. Mechanistic insight into the selective catalytic reduction of NO by NH_3 over α-Fe_2O_3(001): a density functional theory study. *Catal. Sci. Technol.* **2019**, *9*, 116−124.
(37) Sandratskii, L. M.; Uhl, M.; Kübler, J. Band theory for electronic and magnetic properties of α-Fe_2O_3. *J. Phys. Condens. Matter* **1996**, *8*, 983−989.
(38) Tang, J. J.; Liu, B. Reactivity of the Fe_2O_3(0001) surface for methane oxidation: a GGA+ U study. *J. Phys. Chem. C* **2016**, *120*, 6642−6650.
(39) Ding, Y.; Xu, Y.; Song, Y.; Guo, C.; Hu, P. Quantitative studies of the coverage effects on microkinetic simulations for NO Oxidation on Pt (111). *J. Phys. Chem. C* **2019**, *123*, 27594−27602.
(40) Yao, Z.; Guo, C.; Mao, Y.; Hu, P. Quantitative determination of C-C coupling mechanisms and detailed analyses on the activity and selectivity for Fischer-Tropsch synthesis on Co(0001): microkinetic modeling with coverage effects. *ACS Catal.* **2019**, *9*, 5957−5973.
(41) Chen, J. F.; Jia, M. L.; Hu, P.; Wang, H. F. CATKINAS: A Large-Scale Catalytic Microkinetic Analysis Software for Mechanism Auto-Analysis and Catalyst Screening. *J. Comput. Chem.* **2021**, *42*, 379−391.
(42) Chen, J. F.; Jia, M. L.; Lai, Z. Z.; Hu, P.; Wang, H. F. SSIA: A Sensitivity-Supervised Interlock Algorithm for High-Performance Microkinetic Solving. *J. Chem. Phys.* **2021**, *154*, No. 024108.
(43) Chen, J. F.; Mao, Y.; Wang, H. F.; Hu, P. Reversibility Iteration Method for Understanding Reaction Networks and for Solving Microkinetics in Heterogeneous Catalysis. *ACS Catal.* **2016**, *6*, 7078−7087.
(44) Nørskov, J. K.; Bligaard, T.; Logadottir, A.; Kitchin, J. R.; Chen, J. G.; Pandelov, S.; Stimming, U. Trends in the exchange current for hydrogen evolution. *J. Electrochem. Soc.* **2005**, *152*, J23−J26.
(45) Xie, W.; Xu, J.; Chen, J.; Wang, H.; Hu, P. Achieving Theory-Experiment Parity for Activity and Selectivity in Heterogeneous Catalysis Using Microkinetic Modeling. *Accounts Chem. Res.* **2022**, *55*, 1237−1248.
(46) Yuan, H.; Chen, J.; Guo, Y.; Wang, H.; Hu, P. Insight into the superior catalytic activity of MnO_2 for low-content NO oxidation at room temperature. *J. Phys. Chem. C* **2018**, *122*, 25365−25373.
(47) Linstorm, P. NIST chemistry webbook, NIST standard reference database number 69. *J. Phys. Chem. Ref. Data, Monogr. 9* **1998**, 1−1951.

https://doi.org/10.1021/jacsau.2c00424
JACS Au 2022, 2, 2352−2358